

## Precision Lifetime Measurements Using LaBr<sub>3</sub> Detectors With Stable and Radioactive Beams.

P.H.Regan<sup>1,2,a</sup>, Zs.Podolyák<sup>1</sup>, T.Alharbi<sup>3,1</sup>, P.J.R.Mason<sup>1,15</sup>, A.M.Bruce<sup>4</sup>, C.Townsley<sup>1</sup>, O.J.Roberts<sup>4</sup>, N.Mărginean<sup>5</sup>, R.Mărginean<sup>5</sup>, D.Ghită<sup>5</sup>, K.Mullholland<sup>6</sup>, J.F.Smith<sup>6</sup>, R.Britton<sup>1</sup>, Z.Patel<sup>1,16</sup>, M.Nakhostin<sup>1</sup>, S.Rice<sup>1,16</sup>, E.Wilson<sup>1</sup>, N.Alazemi<sup>1</sup>, N.Alkhomashi<sup>7</sup>, D.Bucurescu<sup>5</sup>, G.Cata-Danil<sup>5</sup>, D.Deleanu<sup>5</sup>, D.Filipescu<sup>5</sup>, T.Glodariu<sup>5</sup>, I.Cata-Danil<sup>5</sup>, C.Mihai<sup>5</sup>, A.Negret<sup>5</sup>, C.R.Nita<sup>5</sup>, T.Sava<sup>5</sup>, L.Stroe<sup>5</sup>, G.Suliman<sup>5</sup>, P.Detistov<sup>8</sup>, U.Garg<sup>9</sup>, P.C.Bender<sup>10</sup>, A.Algora<sup>11</sup>, S.Liddick<sup>12</sup>, N.Cooper<sup>13</sup>, V. Werner<sup>13</sup>, S.Lalkovski<sup>14</sup>, S.Kisyov<sup>15</sup>, F.Browne<sup>4,16</sup>, P.-A. Söderström<sup>16</sup>, H. Watanabe<sup>16,18</sup>, and T. Sumikama<sup>17,19</sup>

<sup>1</sup>Department of Physics, University of Surrey, Guildford, GU2 7XH, UK

<sup>2</sup>National Physical Laboratory, Teddington, Middlesex, TW11 0LW, UK

<sup>3</sup>Department of Physics, College of Science in Zulfi, Almajmaah University, PO Box 66, 11952, Saudi Arabia

<sup>4</sup>School of Computing, Engineering and Mathematics, University of Brighton, Brighton, BN2 4GJ, UK

<sup>5</sup>Horia Hulubei National Institute of Physics and Nuclear Engineering (IFIN-HH), RO-077125, Bucharest, Romania

<sup>6</sup>University of the West of Scotland, Paisley, Scotland

<sup>7</sup>KACST, PO Box 6086, Riyadh, 11442, Saudi Arabia

<sup>8</sup>Institute for Nuclear Research and Engineering (IRNE), Bulgarian Academy of Sciences, Sofia, Bulgaria

<sup>9</sup>Department of Physics, University of Notre Dame, Notre Dame, Indiana, 46556, USA

<sup>10</sup>Department of Physics, Florida State University, Tallahassee, Florida, USA

<sup>11</sup>IFIC, CSIC-Universidad de Valencia, A.C. 22085, E 46071, Valencia, Spain

<sup>12</sup>NSCL, Michigan State University, East Lansing, Michigan, 48824, USA

<sup>13</sup>Wright Nuclear Structure Facility, Yale University, New Haven, CT 06520-8120, USA

<sup>14</sup>Faculty of Physics, University of Sofia St Kliment Ohridski, BG-1164 Sofia, Bulgaria

<sup>15</sup>STFC, Daresbury Laboratory, Warrington, UK

<sup>16</sup>RIKEN Nishina Centre, RIKEN, 2-1 Hirosawa, Wako-Shi, Saitama, 351-0198, Japan

<sup>17</sup>Faculty of Science and Technology, Tokyo University of Science, 2461 Yamazaki, Noda, Chiba, 278-8510, Japan

<sup>18</sup>Department of Physics, Beihang University, Beijing 100191, China

<sup>19</sup>Department of Physics, Tohoku University, Aoba, Sendai, Miyagi 980-8578, Japan

**Abstract.** A range of high resolution gamma-ray spectroscopy measurements have been carried out using arrays which include a number of Cerium-doped Lanthanum-Tribromide (LaBr<sub>3</sub>(Ce)) scintillation detectors used in conjunction with high-resolution hyper-pure germanium detectors. Examples of the spectral and temporal responses of such set-ups, using both standard point radioactive sources <sup>152</sup>Eu and <sup>56</sup>Co, and in-beam fusion-evaporation reaction experiments for precision measurements of nuclear excited states in <sup>34</sup>P and <sup>138</sup>Ce are presented. The current and future use of such arrays at existing (EURICA at RIKEN) and future (NUSTAR at FAIR) secondary radioactive beam facilities for precision measurements of excited nuclear state lifetimes in the 10 ps to 10 ns regime are also discussed.

### 1 Introduction

The measurement of electromagnetic transition probabilities from excited nuclear states can provide significant information to test contemporary models of nuclear structure. Such measurements can be compared with predictions of the single-particle make-up of nuclear excited state wavefunctions as predicted in, for example, truncated, valence-restricted shell model descriptions of low-lying nuclear states. These can be used to highlight transitional regions in the Segre chart where the nuclear structure might be explained as evolving from a seniority-

like to a more collective regime (see e.g., [1].) Indeed, even the simplest information on the lifetimes of the first,  $I^\pi = 2^+$  state in even-even nuclei and the corresponding, extracted  $B(E2:2^+ \rightarrow 0^+)$  value can be used to infer evidence of nuclear (quadrupole) collectivity and, in a model dependent way, to extract parameters such as the transition quadrupole moment ( $Q_0$ ) and nuclear deformation,  $\beta_2$  (see e.g., [2].)

One way to extract the electromagnetic reduced matrix elements,  $B(M\lambda)$ , is via the measurement of nuclear excited state lifetimes, where the transition probability,  $T_{fi}(\lambda L)$  for a state decaying from a state with initial spin

<sup>a</sup>e-mail: p.regan@surrey.ac.uk

$J_i$  to a final state with spin  $J_f$ , by a transition of multipole order  $L$ , is given by the expression [3],

$$T_{fi}(\lambda L) = \frac{8\pi(L+1)}{\hbar L((2L+1)!!)^2} \times \left(\frac{E_\gamma}{\hbar c}\right)^{2L+1} \times B(\lambda L : J_i \rightarrow J_f) \quad (1)$$

Excited state lifetimes in nuclei can span many orders of magnitude and therefore need to be determined using a consortium of different experimental techniques depending on the temporal range of the transitions in question, see e.g., [4, 5]. In the simplest method, the time between coincident decays between successive nuclear states can be measured by isolating the discrete gamma-ray transitions which feed into and out of the level of interest.

By determining the average time difference between two successive decays, the average or 'mean' lifetime of the intermediate nuclear state can be obtained directly, using the so called, delayed co-incidence method. The normalised delayed coincidence time distribution is given by the expression [7],

$$F_i(t) = \int_0^\infty P(t-x)f_i(x)dx \quad (2)$$

where  $P$  is the prompt time distribution which describes the response function of the experimental equipment and  $f_i$  is the probability for the decay of the level of interest,  $i$  at time  $x$ . A second, related way of analysing such data is to use the *centroid shift* method which compares the moments of the delayed and prompt response time functions.

Much modern nuclear spectroscopy is performed using arrays of hyper-pure germanium detectors to measure discrete energy gamma rays as they decay from excited states in cascade. The use of such germanium detector arrays is well established and their excellent energy resolution (typically approximately 2 keV FWHM for the full-energy peak from a 1.33 MeV gamma-ray emitted from a  $^{60}\text{Co}$  source) has enabled a wide range of complex nuclear energy level schemes to be disentangled [6]. The direct coincident timing method between excited states in nuclei as measured using coincidence germanium detectors is generally limited to lifetimes of the order of 1 ns ( $10^{-9}$ ) due to the finite time for charge collection to occur in such semiconductor detectors (e.g., [8].)

Faster, direct coincidences between discrete nuclear states can be measured using scintillation detectors such as  $\text{BaF}_2$  [9], but such detectors suffer a much poorer energy resolution compared to germanium and thus are usually only suitable for coincidence measurements between well separated nuclear transitions in spectrum, such as following  $\beta$ -decay to excited states, or for well-separated transitions fed in the decay of long-lived isomeric states.

Over the course of the last decade halide scintillation materials, specifically Lanthanum tri-bromide, doped with cerium ( $\text{LaBr}_3:\text{Ce}$ ) have been developed [10, 11], which show excellent linearity in gamma-ray response and energy resolutions of the order of 2% for full energy peaks at 2 MeV [12]. The relative high light output from these scintillator materials means that their energy resolution, while

**Table 1.** Details of scintillation detectors, information from reference [13]. The  $\text{LaBr}_3$  values assume 10% Cerium doping level. Data taken from reference [13].

Detector	Light Output (photons/MeV)	Principal decay time (ns)
$\text{NaI(Tl)}$	$3.8 \times 10^4$	230
$\text{BaF}_2$	$1.0 \times 10^4$	0.6 ; 620
$\text{LaBr}_3(\text{Ce})$	$8.0 \times 10^4$	16
$\text{CeBr}_3$	$6.8 \times 10^4$	17

not approaching that of germanium, is significantly improved over previous generation scintillation detector materials for gamma-ray spectroscopy, such as barium fluoride  $\text{BaF}_2$  or sodium iodide ( $\text{NaI(Tl)}$ ). The use of such materials has allowed the measurement of lifetimes of excited nuclear states using the delayed coincidence method with  $\text{LaBr}_3$  detectors [14, 16–18]. These measurements range even down to the  $\sim 10$  ps regime so long as the prompt response function of the detectors as a function of gamma-ray full-peak energy is well understood [15]. A summary of the approximate light outputs and timing characteristics for various scintillation materials available for nuclear spectroscopy is given in the table below.

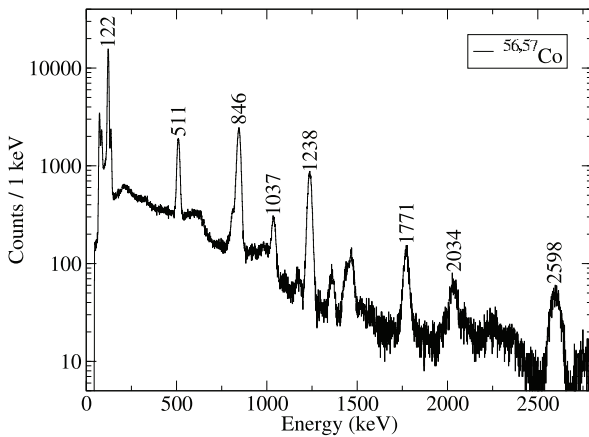
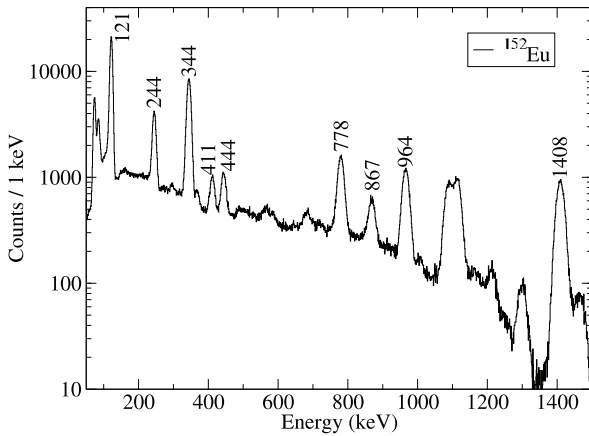
This conference paper presents examples of the performance of arrays of  $\text{LaBr}_3$  detectors using in coincidence to determine lifetimes of nuclear excited states in the  $10^{-11} \rightarrow 10^{-9}$ s regime and presents future plans for the use of a highly modular array of such detectors for use at the focal plane of radioactive beam fragmentation separator devices such as BigRIPS at RIKEN and the SuperFRS at the proposed FAIR facility.

## 2 Detector responses and calibration performances for $^{152}\text{Eu}$ and $^{56}\text{Co}$ point sources.

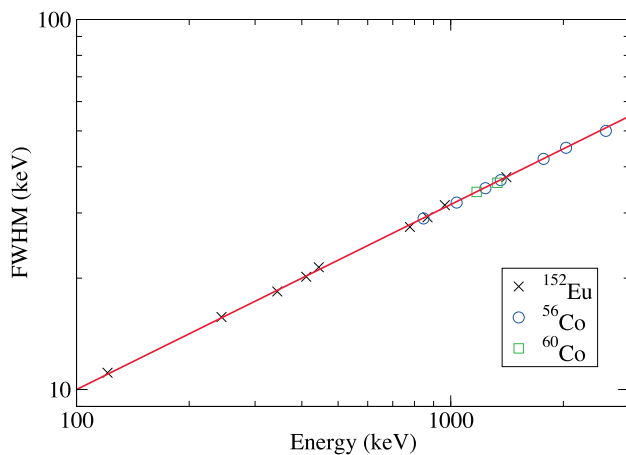
A range of  $\text{LaBr}_3$  detectors have been tested in the current work. In general the detectors used are cylindrical in geometry with diameters of either  $\approx 4$ cm or 5 cm and lengths of 5 cm. Figure 1 shows the energy response of such detectors for discrete line gamma-ray spectroscopy as measured with point sources of  $^{152}\text{Sm}$ , and to test the response in the higher energy range  $^{56}\text{Co}$ .

Figure 2 shows the measured full width at half-maximum (FWHM) for these detectors using the fixed point sources. The response shows a near  $\sqrt{E_\gamma}$  dependence on the FWHM expected for a near Poisson relationship between the light output and the energy deposited by the interacting gamma-rays in the  $\text{LaBr}_3$  crystal.

The timing characteristics of detectors with a diameter of approximately 4 cm and length of 5 cm was also measured using a simple, 'bench-top' coincidence test set-up using a point  $^{152}\text{Eu}$  gamma-ray source to isolate decay transitions in  $^{152}\text{Sm}$ . Coincidence data from this source was taken event by event and the time difference between coincident, full-energy peak transitions was measured (corrected for time walk and the prompt response



**Figure 1.** Examples of LaBr<sub>3</sub> energy spectra from standard radioactive point sources.



**Figure 2.** Measured energy resolution and FWHM of the LaBr<sub>3</sub> detectors over an energy range of 100 keV upto 3 MeV.

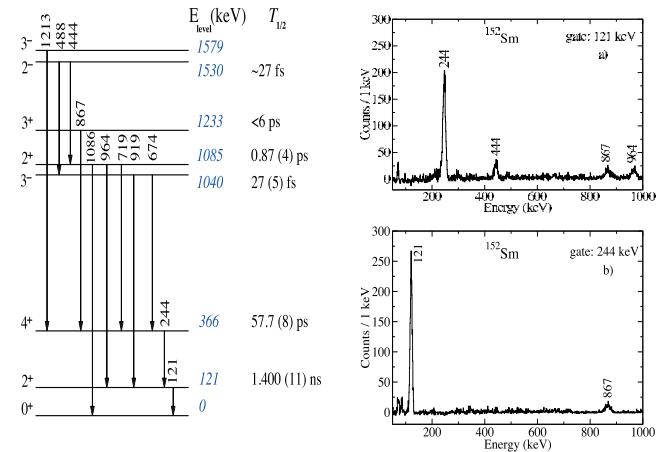


**Figure 3.** Level scheme of <sup>152</sup>Sm (from [19]) and coincidence spectra from <sup>152</sup>Eu source.

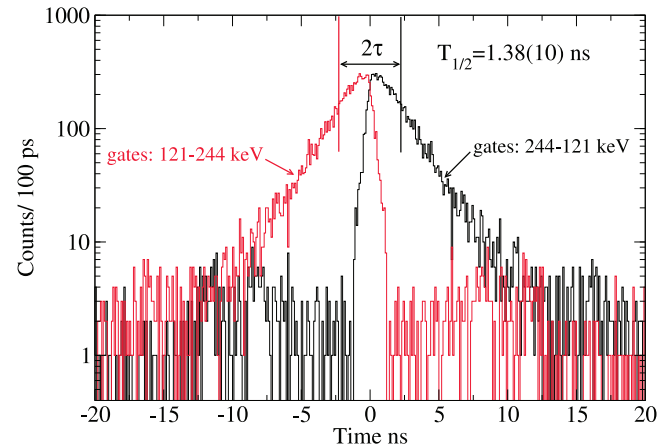


**Figure 4.** Centroid shift values for the lifetime of the yrast  $I^\pi = 2^+$  state in <sup>152</sup>Sm.

of the detector as a function of interacting gamma-ray energy). Figure 3 shows the partial level scheme of <sup>152</sup>Sm as fed in the decay of a <sup>152</sup>Eu point source [19] and the energy gated coincidence spectra gated in the (mutually coincident) 244.7 and 121.8 keV transitions which decay in cascade from the yrast  $I^\pi = 4^+$  state in <sup>152</sup>Sm.

Figure 4 shows the centroid shift (and time reversed centroid shift) of the time-difference spectra associated with the 121.8 and 244.7 keV cascade transitions as measured using the LaBr<sub>3</sub> detectors. The extracted half-life of 1.4 ns is clearly apparent and consistent with the evaluated values for the  $I^\pi = 2^+$  level at 121.8 keV in <sup>152</sup>Sm [19].

### 3 In-beam Experiments at IFIN - Bucharest

A number of in-beam nuclear spectroscopy experiments have been performed using these LaBr<sub>3</sub> detectors at the Tandem Accelerator facility, at IFIN-HH, Bucharest, Romania. These include the selection of: (a) a weakly populated fractional channel (<sup>34</sup>P) in the <sup>18</sup>O+<sup>18</sup>O fusion evaporation reaction [20, 23, 24]; (b) measurement of sub-nanosecond lifetimes in medium and high-spin shell

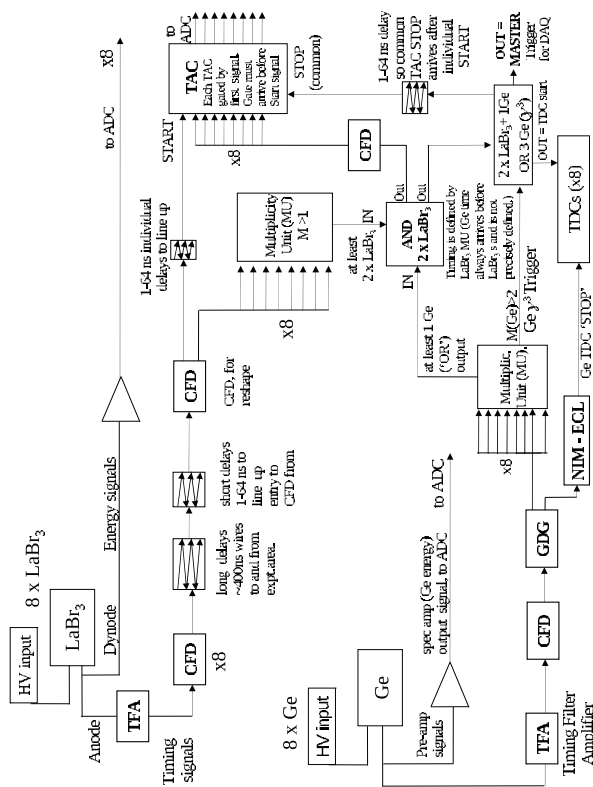


**Figure 5.** Schematic of the signal processing logic used in the Bucharest-based in-beam experiments with combined LaBr<sub>3</sub>-HPGe arrays.

model' states both above and below the  $I^\pi = 10^+$  isomeric state in the N=80 isotope  $^{138}\text{Ce}$  [25]; (c) the use of light-ion ( $^7\text{Li}$ ) induced reactions for measurements of the lifetime of the  $I^\pi = 2^+$  lifetime in the neutron-rich nucleus  $^{188}\text{W}$  populated using the  $^{186}\text{W}(^7\text{Li},\alpha p)^{188}\text{W}$  incomplete fusion reaction [26, 27]; and seniority states in the decay of  $^{132}\text{Te}$  and  $^{134}\text{Xe}$  [28].

The basic experimental set-ups used a mixed array of HPGe and LaBr<sub>3</sub> detectors for measurements of lifetimes down to the tens of picoseconds time regime. The signal processing for the fast-timing part of these measurements was performed using standard NIM electronics using individual time to amplitude converters for each LaBr<sub>3</sub> detector, with a common timing signal for each event being generated by the multiplicity logical coincidence unit. A schematic of the underlying signal processing electronics logic for these experiments is shown in figure 5

### 3.1 Measurement of the lifetime of the yrast $I^\pi = 4^-$ intruder state in $^{34}\text{P}$ .

Figure 6 shows an example of the in-beam gamma-ray coincidence spectra used to identify the main, low-lying yrast cascade in  $^{34}\text{P}$  following its production in the fusion evaporation reaction between an  $^{18}\text{O}$  beam and  $^{18}\text{O}$  target (in the form of an isotopically enriched Tantalum-oxide foil). The nucleus of study in this work,  $^{34}\text{P}$ , was formed via the  $pn$  evaporation channel, which constituted a rather

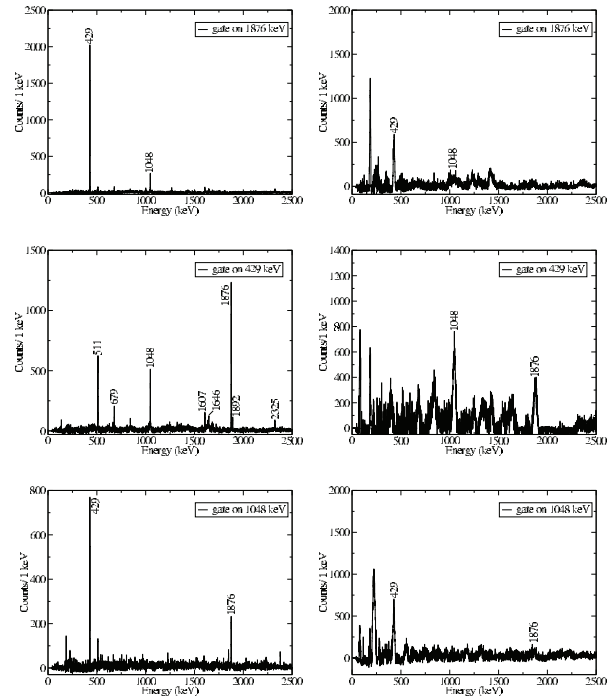


**Figure 6.** Comparison of measured gamma-gamma coincidence spectra gated on transitions in  $^{34}\text{P}$  following the  $^{18}\text{O}+^{18}\text{O}$  fusion evaporation reaction, taken from reference [24].

small fraction of the total fusion-evaporation yield (the order of 10 mb from a total fusion cross-section of the order of at least several hundred mb). The spectra show the power of the coincidence gating mode for the isolation of specific levels via 2-D gating in a 3 dimensional array of  $(E_{\gamma 1}, E_{\gamma 2}, \Delta T)$ , where  $E_{\gamma n}$  are the relevant full energy peaks and  $\Delta T$  is the time difference (as measured in a series of time to amplitude converters) between the arrival of the two coincident energy signals.

Figure 7 shows the partial level scheme for  $^{34}\text{P}$  as published in references [21, 22] using the same fusion-evaporation reaction. Figure 8 shows the time difference spectra between transitions identified in the yrast cascade of  $^{34}\text{P}$  and also, for comparison, from the yrast states in  $^{33}\text{S}$  via the much stronger populated  $3n$  evaporation channel. The time difference spectra between the (background subtracted) coincident LaBr<sub>3</sub> energy gates shows clearly the presence of a state with a half-life of 2 ns, which is associated with the predominantly M2 decay between the yrast spin 4 and  $I^\pi = 2^+$  states in this nucleus. This measurement is consistent with a negative parity for the yrast spin 4 state, which can be explained by the state having a significant neutron  $f_{7/2}$  'intruder' character [23].

### 3.2 Lifetime Studies in the N=80 Nucleus $^{138}\text{Ce}$ .

Excited states in the N=80 nucleus  $^{138}\text{Ce}$  were populated using the  $^{130}\text{Te}(^{12}\text{C},4n)^{138}\text{Ce}$  fusion-evaporation reaction using a 56 MeV beam on a 1 mg/cm<sup>2</sup> isotopically enriched  $^{130}\text{Te}$  target on a 20 mg/cm<sup>2</sup> lead backing. The 4n evaporation channel was the main reaction channel produced

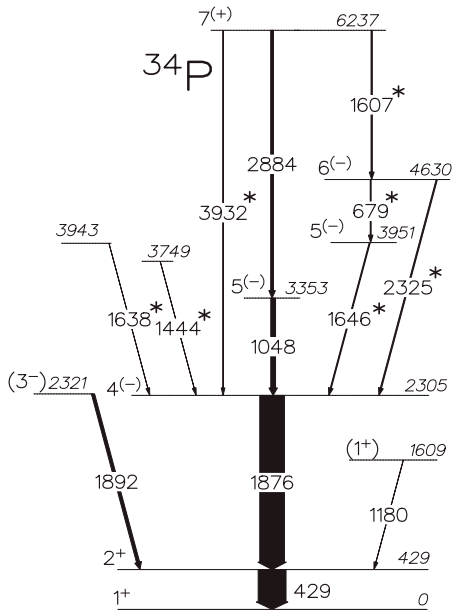


Figure 7. Level scheme of  $^{34}\text{P}$  as observed in the current work, taken from [21].

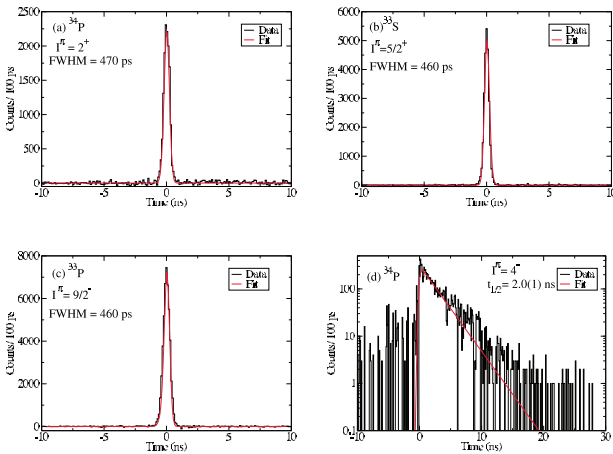


Figure 8. LaBr<sub>3</sub>-LaBr<sub>3</sub> time difference spectra showing the (bottom right) 2 ns half-life of the  $I^\pi = 4^+$  state in  $^{34}\text{P}$ , (taken from reference [24]).

in this reaction with states up to approximately  $20\hbar$  identified. The energy level scheme for the near-yrast states in  $^{138}\text{Ce}$  as identified in the current reaction is consistent with previous studies of this nucleus [30], see figure 9.

Of particular note is the  $I^\pi = 10^+$  isomeric state in this nucleus which has a measured decay half-life of  $81 \pm 2$  ns [31]. The presence of this isomeric state was used to provide additional channel selection in the experiment by separating in time whether discrete gamma-rays measured in the hyperpure germanium detectors in this experiment were measured before (i.e., 'anticipated') or after ('delayed') the fast LaBr<sub>3</sub>-LaBr<sub>3</sub> coincidences in the same 'triples' gamma-ray event. Figure 10 shows the two dimensional matrix of energies measured in the hyper-pure germanium against time difference between these transitions and the LaBr<sub>3</sub> coincidences in the same event. Gat-

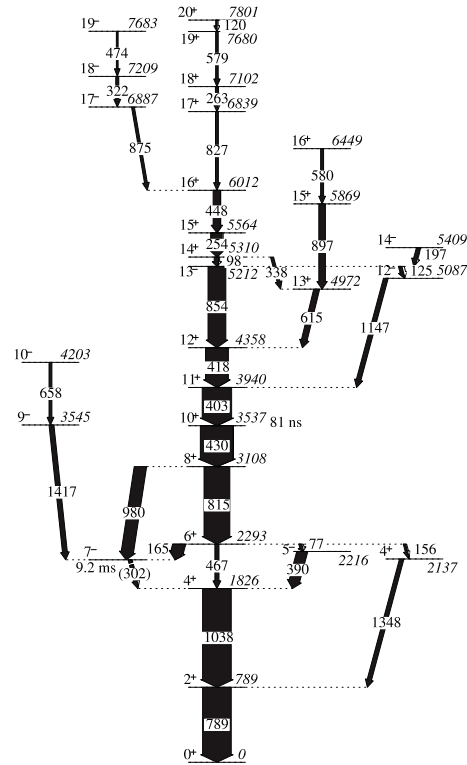


Figure 9. Partial level scheme for the near-yrast states in  $^{138}\text{Ce}$  (taken from reference [24]).

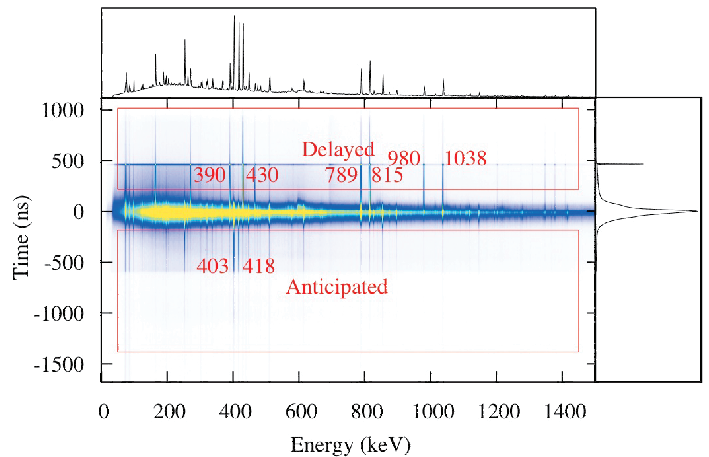


Figure 10. 2-D matrix of germanium energy versus time difference between the master trigger and HPGe signal in the  $^{12}\text{C}+^{130}\text{Te}$  reaction. Note the selection of lines which are before ('anticipated') or following ('delayed') the decay of the  $I^\pi = 10^+$  isomer in this nucleus. Figure from [24].

ing on the different sections of this array allows the selection of transitions either feeding into ('above') or decay out of ('below') the  $I^\pi = 10^+$  isomeric state in this nucleus, as shown in figure 11. This analysis technique and the final experimental results are explained in more detail in reference [25].

The combination of good timing and energy resolutions for the LaBr<sub>3</sub> coincidence technique is highlighted by the measurement of the lifetime of the  $I^\pi = 11^-$  state

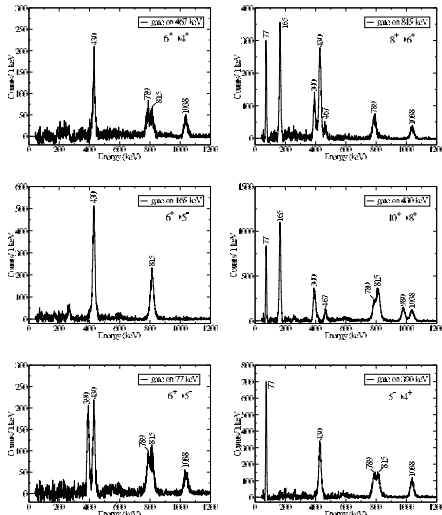


Figure 11. Isomer anticipated gates showing states above and below the  $10^+$  isomer in  $^{138}\text{Ce}$ , from [24].

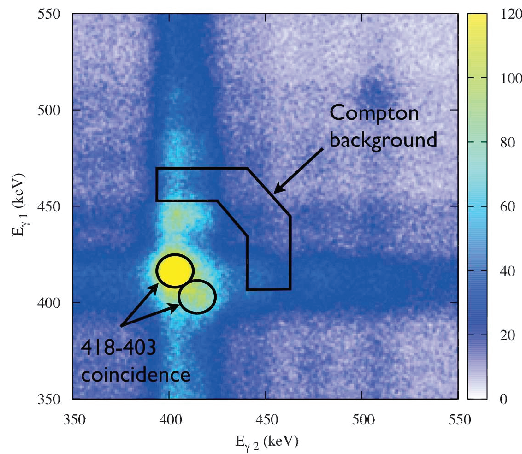


Figure 12. LaBr<sub>3</sub>-LaBr<sub>3</sub> 2-d coincidence energy matrix. The 2-gated regions used for the time difference coincidence between the 418 and 403 keV transitions in  $^{138}\text{Ce}$  are indicated. These were used to isolate the lifetime of the yrast  $I^\pi = 11^+$  state in this nucleus (taken from reference [24]).

in  $^{138}\text{Ce}$  [25]. Figure 12 shows the overview of the germanium gated LaBr<sub>3</sub> energy coincidence matrix for transitions above the  $I^\pi = 10^+$  isomer in  $^{138}\text{Ce}$ .

Note the presence of two close lying lines at energies of 403 and 418 keV which correspond to the discrete transitions which feed into and out of the yrast  $I^\pi = 11^+$  state in this nucleus (see figure 9.) Although these lines are only 15 keV apart in energy, they can be cleanly resolved and their time difference in the LaBr<sub>3</sub> detectors can be determined. This is shown in figure 13 and establishes the mean lifetime of the  $I^\pi = 11^+$  state to be 140(11) ps [25].

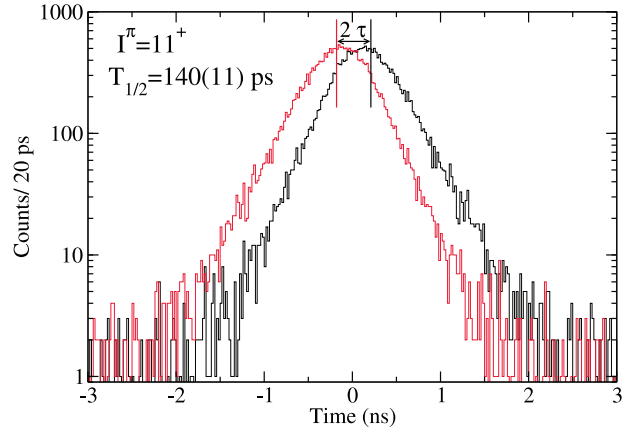


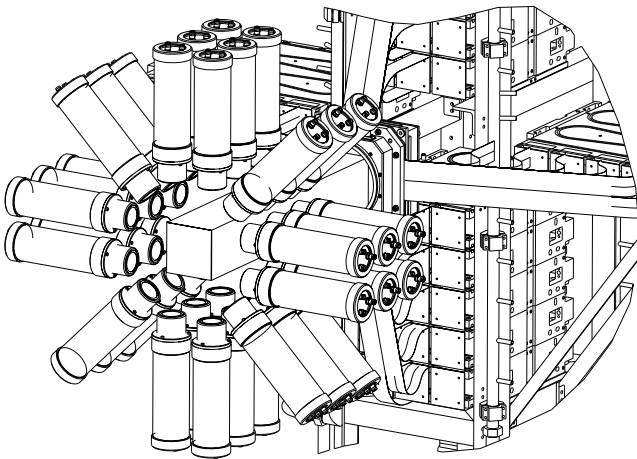
Figure 13. LaBr<sub>3</sub>-LaBr<sub>3</sub> time difference spectra showing the mean lifetime of the  $I^\pi = 11^+$  state in  $^{138}\text{Ce}$ , (taken from reference [24]).



Figure 14. Photograph of encased 2'' x 1.5'' LaBr<sub>3</sub> detector with PMT attached.

#### 4 A Fast-Timing Array for DESPEC at FAIR.

An array of LaBr<sub>3</sub> detectors in a high-efficiency, high granularity 'cross-box' configuration for use the focal plane of the future Super Fragment Separator (SFRS) within the NUSTAR collaboration at the Facility for Anti-proton and Ion Research (FAIR) has been designed and is currently under construction [29]. The proposed array will consist of thirty-six 1.5 inch diameter by 2 inch long LaBr<sub>3</sub> crystals which surround the final focal plane of the SFRS in a box configuration. Figure 14 shows a photograph of such a detector, which includes the photomultiplier tube encased in a mu-metal shield.



**Figure 15.** Design drawing of the 36 detector LaBr<sub>3</sub> fast-timing array configuration surrounding the focal plane of the Super Fragment Separator at GSI.

Figure 15 shows a CAD drawing of the proposed array, which takes up three rows of a 'cross-box' configuration surrounding the final focal plane position at the SFRS. The proposed array is envisaged to surround the AIDA active stopper which will be used to identify the position and decay of radioactive species at the focal plane of the SFRS.

#### 4.1 At RIBF for use in EURICA at RIKEN

Eighteen of the LaBr<sub>3</sub> detectors which will be used in the proposed fast-timing array for FAIR have already been tested in the EURICA gamma-ray array [32, 33]. This combined LaBr<sub>3</sub> hyper-pure germanium array is based at the focal plane of the BigRIPS separator for decay studies of exotic nuclei at the RIBF facility in RIKEN, Japan. The current implementation allows a mixed Ge-LaBr<sub>3</sub> focal plane array which consists of twelve, 7-element germanium 'cluster' detectors, with 18 of the 1.5"×2" LaBr<sub>3</sub> detectors added to provide some rudimentary fast-timing measurements to compare with the data obtained from the superior energy resolution germanium channels. Figure 16 shows a CAD drawing of one half of the EURICA set-up showing the positions of the 18 LaBr<sub>3</sub> detectors in this experimental configuration.

This array has been used in a range of recent experiments, in particular to study the decay from isomers and beta-decay products in neutron-rich fission fragments around  $A \sim 105, 130$  and 160. Initial results include identification and measurement of the lifetime of the  $J^\pi = 2^+$  state in the neutron-rich <sup>104</sup>Zr nucleus using the LaBr<sub>3</sub> detectors in this array [34].

## 5 Summary and Future Directions.

An experimental programme of studies of a range of internal nuclear state lifetimes in the tens of picoseconds to few nanoseconds regime has been undertaken. The main engine for such measurements has been the use of discrete-line coincident spectroscopy between signals measured

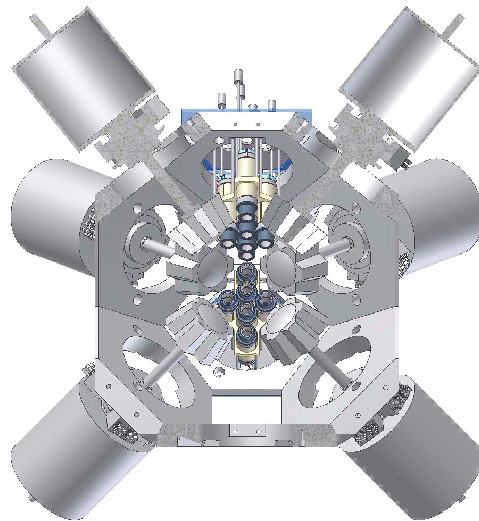


**Figure 16.** Drawing of the 18 LaBr<sub>3</sub> detectors housed in the EURICA array at the focal plane of the BigRIPS spectrometer at RIKEN.

in LaBr<sub>3</sub> gamma-ray detectors, which are shown to couple excellent timing capabilities with acceptable energy resolution for in-beam spectroscopic studies of nuclear structure. To date, most studies have been undertaken using a 'mixed' array combining both LaBr<sub>3</sub> and high-resolution germanium detectors (for specific channel selection). Future programmes include the utilisation of a compact, high-efficiency array of LaBr<sub>3</sub> detectors as part of the DESPEC-FATIMA collaboration within the NUSTAR project at FAIR. Detectors from this array are already being used in commissioning experiments, including for studies of decays from exotic, secondary radioactive beam at fragmentation facilities such as RIBF at RIKEN. Future directions of this work might include investigation of the use of other Halide scintillation materials, such as CeBr<sub>3</sub> [13, 35], which although having a poorer energy resolution compared to LaBr<sub>3</sub> has similar timing properties and operates without the internal 'background' radiation present from the primordial <sup>138</sup>La decay which is intrinsic to the LaBr<sub>3</sub> detectors.

**Acknowledgements** This work is supported by the UK Science and Technology Facilities Council (STFC), the Romanian Ministry for Education and Research [Contracts Module3-24EU-ISOLDE and PN-II-ID-PCE-2011-3-0367(UEFISCDI)], ANCS (Romania) and the US National Science Foundation (Grants No. PHY07-58100, No. PHY-1068192, and No. PHY-07-56474). Almajmaah University (Saudi Arabia), the DMU02/1 contract with the Bulgarian Science Fund, the Bulgarian-Romanian partnership Contracts No. BRS-07/23 and No. 460/PNII Module III, and the U.S. DOE under Grants No. DE-FG02-91ER40609 and No. FPA2008-06419-C02-01.

## References

- [1] J.J.Ressler et al., Phys. Rev. C **69**, 034317 (2004)

- [2] R.F.Casten, Nuclear Structure from a Simple Perspective, p 217ff. ;
- [3] Introductory Nuclear Physics, Kenneth S.Krane, John Wiley and Sons, p 331 (1998) New York
- [4] A.Z.Schwarzschild and E.K.Warburton, Ann. Rev. Nucl. Sci. **18**, 265 (1968)
- [5] P.J.Nolan and J.F.Sharpey-Schafer, Phys. Rep. **42**,1 (1979)
- [6] J.Eberth and J.Simpson, Prog. Part. Nucl. Phys. **60**, 283 (2008)
- [7] T.D.Newton, Phys. Rev. **78**, 490 (1950)
- [8] O.Möller et al., Phys. Rev. **72**, 034306 (2005)
- [9] H.Mach, J. Physics G: Nucl. Part. Phys., **31**, S1421 (2005)
- [10] E.V.D van Loef et al., Nucl. Inst. Meth. Phys. Res. **486**, 254 (2002)
- [11] M.S. Alekhin et al., Applied Physics Letters **102**, 161915 (2013)
- [12] M. Cimela et al., Nucl. Inst. Meth. Phys. Res. **608**, 76 (2009)
- [13] W.M.Higgins et al., Journal of Crystal Growth **310**, 2085 (2008)
- [14] D.L. Smith et al., Physical Review **C77**, 014309 (2008)
- [15] J.M. Regis et al., Nucl. Inst. Meth. Phys. Res. **662**, 82 (2010)
- [16] N. Marginean et al., Eur. Phys. J. **A46**, 329 (2010)
- [17] S.Kisyov et al., Phys. Rev. **C84**, 014324 (2011)
- [18] V.Werner et al., J. Phys: Conf. Ser. **312**, 092062 (2011)
- [19] National Nuclear Data Centre, [www.nndc.bnl.gov](http://www.nndc.bnl.gov)
- [20] T.Alharbi et al., App. Rad. and Isot. **70**, 1337 (2012)
- [21] P.C.Bender et al., Phys. Rev. **C85**, 044305 (2012); *ibid* Phys. Rev. **C80**, 014302 (2009)
- [22] R. Chakrabarti et al., Phys. Rev. **C80**, 034326 (2009)
- [23] P.J. Mason et al., Phys. Rev. **C85**, 064303 (2012)
- [24] T. Alharbi, PhD thesis, University of Surrey, UK (2013)
- [25] T. Alharbi et al., Phys. Rev. **C87**, 104323 (2013)
- [26] P.J.R. Mason et al., *in press*, Phys. Rev C
- [27] P.J.R. Mason et al., AIP Conf. Procs. **1491**, 93 (2012)
- [28] O. Roberts et al., Acta Phys. Pol. **B44**, 403 (2013)
- [29] O. Roberts et al., submitted to Nucl. Inst. Meth. Phys. Res. and these proceedings.
- [30] S.J. Zhu et al., Chin. Phys. Lett. **16**, 635 (1999)
- [31] G. LoBianco et al., Z. Phys. **A318**, 195 (1984)
- [32] S. Nishimura, Prog. Theor. Exp. Phys. 03C006 (2012)
- [33] P.-A Söderström, et al., Nucl. Inst. Meth. B, in print, DOI: 10.1016/j.nimb.2013.03.018.
- [34] F.Browne, A.M.Bruce, T.Sumikama et al., *unpublished*.
- [35] L. Fraille et al., Nucl. Inst. Meth. Phys. Res. **A701**, 235 (2013)